

Nuclear magnetic relaxation rate in a noncentrosymmetric superconductor

N. Hayashi,¹ K. Wakabayashi,^{1,2} P. A. Frigeri,¹ and M. Sigrist¹

¹*Institut für Theoretische Physik, ETH-Hönggerberg, CH-8093 Zürich, Switzerland*

²*Department of Quantum Matter Science, Graduate School of Advanced Sciences of Matter (ADSM), Hiroshima University, Higashi-Hiroshima 739-8530, Japan*

(Received 7 April 2005; revised manuscript received 10 January 2006; published 17 March 2006)

Noncentrosymmetric superconductors possess, in general, order parameters of mixed parity, i.e., the Cooper pairing state consists of spin-singlet and spin-triplet pairing components. We show that this property has important implications for the NMR and other measurable quantities in the heavy Fermion superconductor CePt₃Si. The aspect of parity mixing explains the apparently contradicting observations of a Hebel-Slichter peak in the nuclear spin-lattice relaxation rate T_1^{-1} and the presence of power law in the low-temperature behavior of certain physical quantities, indicating line nodes in the quasiparticle gap.

DOI: [10.1103/PhysRevB.73.092508](https://doi.org/10.1103/PhysRevB.73.092508)

PACS number(s): 74.20.Rp, 74.70.Tx, 76.60.-k

Inversion is one of the key symmetries for the formation of Cooper pairs in superconductors. Unusual properties are expected in superconductors whose crystal structure does not possess an inversion center (e.g., Refs. 1–5, and references therein). For this reason, the recent discovery of superconductivity in the noncentrosymmetric heavy fermion compound CePt₃Si has initiated much excitement.^{6–8} On a microscopic level, the appearance of antisymmetric spin-orbit coupling (ASOC) due to the noncentrosymmetry imprints a characteristic spin structure on the band structure by lifting the usual spin degeneracy.^{9,10} For superconductivity, the lack of inversion symmetry makes the standard labeling of Cooper pairing states by even parity (spin singlet) and odd parity (spin triplet) inapplicable, and it yields parity mixing, in general.² The modification of the band structure and the parity mixing are likely responsible for the surprisingly high value of the upper critical field H_{c2} in CePt₃Si, which significantly exceeds the standard paramagnetic limit.^{3,6,8,11,12} Moreover, nuclear magnetic resonance (NMR) experiments display apparently incompatible features. The nuclear spin-lattice relaxation rate T_1^{-1} has a Hebel-Slichter peak just below the onset of superconductivity, usually a sign of *conventional* superconductivity. In contrast, *unconventional* superconductivity is suggested by the low-temperature power-law behavior of T_1^{-1} , indicating line nodes in the quasiparticle gap.^{8,13,14} The presence of line nodes is also supported by London penetration depth measurements^{8,15} as well as the thermal conductivity experiments.¹⁶ Therefore, an important task is to reconcile the mutually contradicting experimental results in a consistent picture.

In the present study, we demonstrate that the key to resolving this puzzle lies in the parity mixing of pairing states as a natural consequence of the lack of inversion symmetry in this material. This aspect can be implemented by considering a two-component order parameter with spin-singlet and spin-triplet components. In this model, the Hebel-Slichter peak relies on the presence of a finite coherence effect. A sufficient condition for it is that the spin-singlet component incorporates a gap function with a finite average on the Fermi surface $\langle \psi(\mathbf{k}) \rangle \neq 0$, most easily satisfied by a conventional (isotropic) *s*-wave pairing state. The line nodes

appear as a consequence of the superposition of the two components.¹⁷

Our analysis is based on the single-particle Hamiltonian³

$$\mathcal{H} = \sum_{k,s} \xi_k c_{ks}^\dagger c_{ks} + \alpha \sum_{k,s,s'} \boldsymbol{\lambda}_k \cdot [c_{ks}^\dagger \boldsymbol{\sigma}_{ss'} c_{ks'}]. \quad (1)$$

ξ_k is the band energy measured relative to the chemical potential. The second term describes the ASOC with $\boldsymbol{\lambda}_k = -\boldsymbol{\lambda}_{-k}$ and α as the coupling constant. [$c_{ks}^{(\dagger)}$ annihilates (creates) an electron with momentum \mathbf{k} and spin s .] The ASOC term vanishes for systems with an inversion center. On the basis of symmetry arguments, the crystal symmetry ($P4mm$) of CePt₃Si yields

$$\boldsymbol{\lambda}_k = \sqrt{\frac{3}{2}} \frac{1}{k_F} (-k_y, k_x, 0), \quad (2)$$

in the lowest-order expansion, assuming a spherical Fermi surface where $\boldsymbol{\lambda}_k$ is normalized such that the average over the Fermi surface $\langle |\boldsymbol{\lambda}_k|^2 \rangle = 1$.³ k_F is the Fermi wave number for $\alpha=0$.

Starting from the basic tetragonal symmetry of CePt₃Si ignoring the ASOC in Eq. (1), we could classify all basic pairing states, distinguishing the spin-singlet and spin-triplet states.^{3,5} A general argument by Anderson¹⁸ shows that inversion symmetry is essential to realize spin-triplet pairing. Hence, spin-triplet pairing states are expected to be suppressed when the ASOC is turned on. A careful examination leads, however, to the conclusion that a certain set of triplet pairing states remains stable even when $\alpha \neq 0$. These states are characterized by the \mathbf{d} vector $\mathbf{d}_k \parallel \boldsymbol{\lambda}_k$.³ In addition, the ASOC mixes even-parity spin-singlet and odd-parity spin-triplet pairing components. Interestingly, the conventional *s*-wave spin-singlet pairing state mixes with the state corresponding to $\mathbf{d}_k = \boldsymbol{\lambda}_k$, which has under these symmetry conditions the highest possible symmetry, corresponding to the trivial representation of the generating point group $C_{4v}A_1$.¹⁷

The A_1 -superconducting phase has a gap function of the form

$$\hat{\Delta}_k = (\Psi \hat{\sigma}_0 + \mathbf{d}_k \cdot \hat{\boldsymbol{\sigma}}) i \hat{\sigma}_y = [\Psi \hat{\sigma}_0 + \Delta(-\tilde{k}_y \hat{\sigma}_x + \tilde{k}_x \hat{\sigma}_y)] i \hat{\sigma}_y, \quad (3)$$

with the s -wave pairing component Ψ and the \mathbf{d} vector $\mathbf{d}_k = \Delta(-\tilde{k}_y, \tilde{k}_x, 0)$. The unit vector $\tilde{\mathbf{k}} = (\tilde{k}_x, \tilde{k}_y, \tilde{k}_z) = (\cos \phi \sin \theta, \sin \phi \sin \theta, \cos \theta)$.

For our discussion, we will use the quasi-classical theory of superconductivity.^{19–21} In this formulation, we concentrate on the states in the immediate vicinity of the Fermi surface and assume $|\Psi|, |\Delta|, \alpha \ll \varepsilon_F$ (ε_F is the Fermi energy). The quasiclassical Green's function \check{g} can be written as a matrix in Nambu (particle-hole) space,

$$\check{g}(\mathbf{r}, \tilde{\mathbf{k}}, i\omega_n) = -i\pi \begin{pmatrix} \hat{g} & i\hat{f} \\ -i\hat{f} & -\hat{g} \end{pmatrix}. \quad (4)$$

The vector \mathbf{r} is the real-space coordinate, the unit vector $\tilde{\mathbf{k}}$ indicates the position on the spherical Fermi surface, and $\omega_n = \pi T(2n+1)$ is the Matsubara frequency. Throughout the paper, “hat” $\hat{\cdot}$ denotes the 2×2 matrix in the spin space, and “check” $\check{\cdot}$ denotes the 4×4 matrix composed of the 2×2 Nambu space and the 2×2 spin space. The Eilenberger equation, which includes the spin-orbit coupling [Eq. (2)], is given by^{22–25}

$$i\mathbf{v}_F \cdot \nabla \check{g} + [i\omega_n \check{\tau}_3 - \alpha \check{\boldsymbol{\lambda}}_k \cdot \check{\mathbf{S}} - \check{\Delta}_k, \check{g}] = 0, \quad (5)$$

with

$$\check{\tau}_3 = \begin{pmatrix} \hat{\sigma}_0 & 0 \\ 0 & -\hat{\sigma}_0 \end{pmatrix}, \quad \check{\mathbf{S}} = \begin{pmatrix} \hat{\boldsymbol{\sigma}} & 0 \\ 0 & \hat{\boldsymbol{\sigma}}^r \end{pmatrix}, \quad (6)$$

$$\check{\boldsymbol{\lambda}}_k = \begin{pmatrix} \boldsymbol{\lambda}_k \hat{\sigma}_0 & 0 \\ 0 & \boldsymbol{\lambda}_{-k} \hat{\sigma}_0 \end{pmatrix} = \begin{pmatrix} \boldsymbol{\lambda}_k \hat{\sigma}_0 & 0 \\ 0 & -\boldsymbol{\lambda}_k \hat{\sigma}_0 \end{pmatrix}, \quad (7)$$

$$\boldsymbol{\lambda}_k = \sqrt{\frac{3}{2}}(-\tilde{k}_y, \tilde{k}_x, 0), \quad (8)$$

$$\check{\Delta}_k = \begin{pmatrix} 0 & \hat{\Delta}_k \\ -\hat{\Delta}_k^\dagger & 0 \end{pmatrix}. \quad (9)$$

Here, $\hat{\boldsymbol{\sigma}} = (\hat{\sigma}_x, \hat{\sigma}_y, \hat{\sigma}_z)$ is the Pauli matrix, $\hat{\sigma}_0$ is the unit matrix, $\hat{\boldsymbol{\sigma}}^r = -\hat{\sigma}_y \hat{\boldsymbol{\sigma}} \hat{\sigma}_y$, \mathbf{v}_F is the Fermi velocity, and $[\check{a}, \check{b}] = \check{a}\check{b} - \check{b}\check{a}$. We use units in which $\hbar = k_B = 1$. The Eilenberger equation is supplemented by the normalization condition, $\check{g}^2 = -\pi^2 \check{1}$.^{19,22}

With the pairing state in Eq. (3) and the spin-orbit coupling in Eq. (8), we obtain the following Green's functions from the Eilenberger equation (5) and the normalization condition,²⁶

$$\hat{g} = g_I \hat{\sigma}_I + g_{II} \hat{\sigma}_{II}, \quad \hat{g} = -\hat{\sigma}_y (\bar{g}_I \hat{\sigma}_I + \bar{g}_{II} \hat{\sigma}_{II}) \hat{\sigma}_y,$$

$$\hat{f} = (f_I \hat{\sigma}_I + f_{II} \hat{\sigma}_{II}) i \hat{\sigma}_y, \quad \hat{f} = -i \hat{\sigma}_y (\bar{f}_I \hat{\sigma}_I + \bar{f}_{II} \hat{\sigma}_{II}), \quad (10)$$

with the matrices $\hat{\sigma}_{I,II}$ defined by^{1,17,27} $\hat{\sigma}_{I,II} = (\hat{\sigma}_0 \pm \bar{\boldsymbol{\lambda}}_k \cdot \hat{\boldsymbol{\sigma}})/2$ and $\bar{\boldsymbol{\lambda}}_k = (-\bar{k}_y, \bar{k}_x, 0)$, where $\bar{\mathbf{k}} = (\bar{k}_x, \bar{k}_y, 0) = (\cos \phi, \sin \phi, 0)$. In the case of a spatially uniform system,²⁶

$$g_{I,II} = \frac{\omega_n}{B_{I,II}}, \quad \bar{g}_{I,II} = \frac{-\omega_n}{B_{I,II}}, \quad (11a)$$

$$f_{I,II} = \frac{\Psi \pm \Delta \sin \theta}{B_{I,II}}, \quad \bar{f}_{I,II} = \frac{\Psi^* \pm \Delta^* \sin \theta}{B_{I,II}}. \quad (11b)$$

The denominators $B_{I,II}$ are given as $B_{I,II} = \sqrt{\omega_n^2 + |\Psi \pm \Delta \sin \theta|^2}$, and the signs in front of the square root are determined by the condition, $\text{sgn}(\text{Re}\{g_{I,II}\}) = \text{sgn}(\text{Re}\{\omega_n\})$. Note that the Green's functions [Eq. (11)] do not explicitly depend on the spin-orbit coupling constant α , although α is kept nonzero. This result of the Eilenberger equation reflects the fact that the spin-triplet component contained in the pairing state [Eq. (3)] is not affected by the ASOC of Eq. (2).³ In this way, the quasi-classical formulation incorporates the effect of noncentrosymmetry in a very convenient form, which may prove beneficial also for future studies.

Nevertheless, the Green's functions labeled by the indices I and II belong to the two distinct Fermi surfaces, which are split by the spin-degeneracy lifting due to the ASOC.^{1,17,26,27} The quasiparticle gap is different on the two Fermi surfaces: $\Delta_{I\tilde{\mathbf{k}}} = |\Psi + \Delta \sin \theta|$ and $\Delta_{II\tilde{\mathbf{k}}} = |\Psi - \Delta \sin \theta|$. The densities of states on the two Fermi surfaces are also different, in general, and this difference has important implications in various other contexts. However, we choose them to be equal here for simplicity, since our results would be on a qualitative level insensitive to this detail.

The pairing interaction leading to the gap function [Eq. (3)] is characterized by three coupling constants, λ_s , λ_t , and λ_m . Here, λ_s and λ_t result from the pairing interaction within each spin channel (s : singlet, t : triplet). λ_m is the scattering of Cooper pairs between those two parity channels, present in systems without inversion symmetry.¹⁷ The gap equations are written as

$$\Psi = \lambda_s \pi T \sum_{|\omega_n| < \omega_c} \langle f_+ \rangle + \lambda_m \pi T \sum_{|\omega_n| < \omega_c} \langle \sin \theta f_- \rangle, \quad (12)$$

$$\Delta = \lambda_t \pi T \sum_{|\omega_n| < \omega_c} \langle \sin \theta f_- \rangle + \lambda_m \pi T \sum_{|\omega_n| < \omega_c} \langle f_+ \rangle, \quad (13)$$

where $f_{\pm} = (f_I \pm f_{II})/2$ and ω_c is the cutoff energy. The angular brackets denote the average over the Fermi surface, assuming the spherical Fermi surface for simplicity. In the limit $T \rightarrow T_c$ (T_c : the superconducting critical temperature), the linearized gap equations allow us to determine λ_t and λ_s by

$$\lambda_t = \frac{3}{2} \left(\frac{1}{w} - \nu \lambda_m \right), \quad \lambda_s = \frac{2}{3} \lambda_t + \left(\nu - \frac{2}{3\nu} \right) \lambda_m, \quad (14)$$

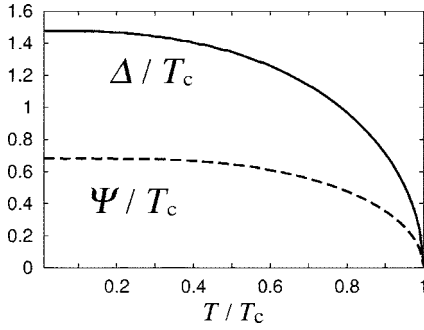


FIG. 1. The temperature dependence of the order parameters in units of T_c . The spin-triplet component Δ (solid line) and the spin-singlet s -wave component Ψ (dashed line). $\omega_c=20T_c$, $\lambda_m=0.12$, and $\nu=0.5$. Both Δ and Ψ are real and positive.

$$w = \ln\left(\frac{T}{T_c}\right) + \sum_{0 \leq n < (\omega_c/\pi T - 1)/2} \frac{2}{2n+1}, \quad (15)$$

if the parameters λ_m and $\nu \equiv (\Psi/\Delta)|_{T \rightarrow T_c - 0^+}$ are given.

In Fig. 1, we show the temperature dependence of the order parameters Δ and Ψ obtained from the gap equations [Eqs. (12) and (13)]. We set $\omega_c=20T_c$, $\lambda_m=0.12$, and $\nu=0.5$, yielding $\lambda_t \approx 0.39$ and $\lambda_s \approx 0.16$. When Δ is fixed to be real and positive without loss of generality, such a solution as Ψ is also real and positive, is stable for the above parameters.

We turn now to the nuclear spin-lattice relaxation rate $1/T_1$. Assuming for the NMR experiment a static magnetic field in the z direction, we arrive at the following expression for $1/T_1$ in terms of the quasi-classical Green's function \check{g} :²⁸

$$\frac{T_1(T_c)T_c}{T_1(T)T} = \frac{1}{4T} \int_{-\infty}^{\infty} \frac{d\omega}{\cosh^2(\omega/2T)} W(\omega), \quad (16)$$

with

$$W(\omega) = \langle a_{\uparrow\downarrow}^{22}(\omega) \rangle \langle a_{\uparrow\uparrow}^{11}(-\omega) \rangle - \langle a_{\uparrow\uparrow}^{21}(\omega) \rangle \langle a_{\uparrow\downarrow}^{12}(-\omega) \rangle, \quad (17)$$

$$\check{a}(\omega) = \frac{i}{2\pi} \check{\tau}_3 [\check{g}(i\omega_n \rightarrow \omega + i\eta) - \check{g}(i\omega_n \rightarrow \omega - i\eta)], \quad (18)$$

$$\check{a} = \begin{pmatrix} \hat{a}^{11} & \hat{a}^{12} \\ \hat{a}^{21} & \hat{a}^{22} \end{pmatrix}, \quad \hat{a}^{ij} = \begin{pmatrix} a_{\uparrow\uparrow}^{ij} & a_{\uparrow\downarrow}^{ij} \\ a_{\downarrow\uparrow}^{ij} & a_{\downarrow\downarrow}^{ij} \end{pmatrix}, \quad (19)$$

where $\eta(>0)$ is an infinitesimally small constant, and we set $\eta=10^{-4}T_c$.

In Fig. 2(a), we show the temperature dependence of $1/T_1T$ obtained from Eq. (16), where the Green's functions in Eqs. (10) and (11) are substituted into $W(\omega)$ [Eq. (17)] through Eqs. (4) and (18). The temperature dependence of Ψ and Δ is obtained from the gap equations as shown in Fig. 1. Obviously, $1/T_1T$ (solid line) possesses a peak just below T_c . In order to identify the origin of this peak, in Fig. 2(a) we plot the contributions of the two terms in Eq. (17) separately: $W = W_{GG} + W_{FF}$,

$$W_{GG}(\omega) = \langle a_{\uparrow\downarrow}^{22}(\omega) \rangle \langle a_{\uparrow\uparrow}^{11}(-\omega) \rangle, \quad (20)$$

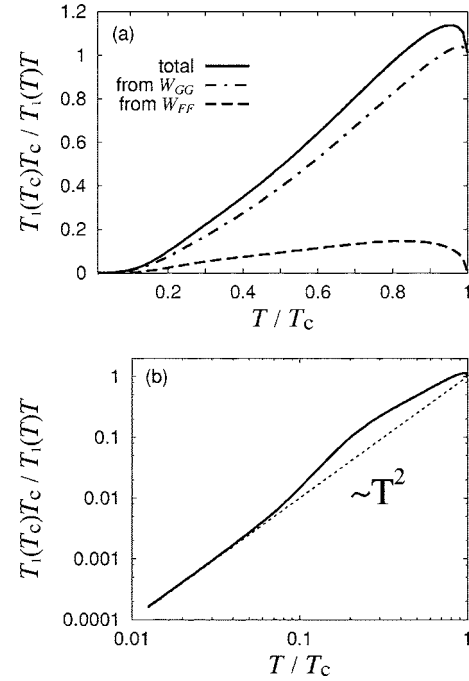


FIG. 2. Temperature dependence of the nuclear spin-lattice relaxation rate $1/T_1T$ (solid lines), $\eta=10^{-4}T_c$. (a) Dashed line is the contribution of the anomalous Green's functions W_{FF} related to the coherence effect. Dashed-dotted line is the contribution of the regular Green's functions W_{GG} related to the density of states. (b) Plot of the same data on a double-logarithmic scale. Dotted line is a plot of T^2 . From the plot, it is noted that T_1^{-1} follows the T^3 law at low temperatures.

$$W_{FF}(\omega) = -\langle a_{\uparrow\uparrow}^{21}(\omega) \rangle \langle a_{\uparrow\downarrow}^{12}(-\omega) \rangle. \quad (21)$$

W_{GG} and W_{FF} are composed of the regular Green's functions and the anomalous Green's functions, respectively. The coherence factor is represented as $1 + W_{FF}/W_{GG}$. The contribution of W_{FF} (dashed line) is related to the coherence effect and gives the dominant contribution to the peak below T_c as seen in Fig. 2(a). W_{FF} is finite owing to the s -wave component Ψ . In contrast, W_{GG} (dashed-dotted line) describes the contribution of the density of states and its temperature-dependent variation. The contribution to the peak from the singularity of the density of states at the gap edge is minor, since this singularity is rather weak due to the anisotropy of the gaps $|\Psi \pm \Delta \sin \theta|$ on both Fermi surfaces I and II. Therefore, the peak in the total $1/T_1T$ (solid line) can clearly be attributed to the coherence-factor-induced enhancement of the relaxation rate T_1^{-1} originated from the coherence effect under the favor of nonzero contribution of W_{FF} .

Turning to the low-temperature behavior, we present the same data on a double-logarithmic scale in Fig. 2(b). The temperature dependence of $1/T_1T$ exhibits a T^2 power law at low temperatures, characteristic of the presence of line nodes in the gap. These nodes are the result of the superposition of spin-singlet and spin-triplet contributions (each separately would not produce line nodes). On the Fermi surface I, the gap is $|\Psi + \Delta \sin \theta|$ and is nodeless, referring to Eq. (11b), (note that $\Psi > 0$, $\Delta > 0$, and $0 \leq \theta \leq \pi$). On the other hand, the form of the gap on the Fermi surface II is $|\Psi - \Delta \sin \theta|$,

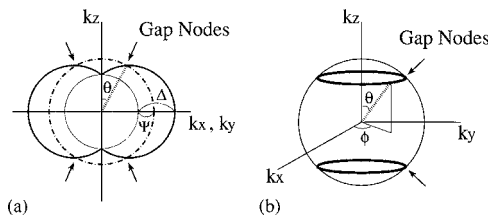


FIG. 3. Schematic figures of the gap structure on the Fermi surface. (a) Cross section of the Fermi surface, showing the places of gap nodes at which the gap $|\Psi - \Delta \sin \theta| = 0$. (b) Line nodes of the gap in the three-dimensional \mathbf{k} space.

where nodes can appear for $\Psi < \Delta$ (see Fig. 3). These line nodes on the Fermi surface II lead to the low-temperature T^3 law in T_1^{-1} (i.e., T^2 in $1/T_1 T$) as shown in Fig. 2(b), which is in qualitative agreement with the experimental result. Moreover, the power laws observed in the London penetration depth^{8,15,26} and the thermal conductivity¹⁶ are also consistent with this gap form.

In conclusion, the apparent puzzle found in the temperature dependence of the NMR relaxation rate¹³ may turn out to be a key experiment to determine the pairing symmetry. The presence of a Hebel-Slichter peak can only be attributed to a coherence effect that points toward a conventional s -wave-like pairing. On the other hand, the low-temperature power-law behavior observed in a variety of experiments¹³⁻¹⁶ indicates the presence of a line node in the quasiparticle gap. In this paper, we have shown that this discrepancy can be explained by including the natural parity mixing of the Cooper pairing states as given in Eq. (3). The symmetry of the odd-parity spin-triplet part is uniquely defined by the form of

the ASOC. That $s+p$ -wave pairing state is also compatible with other experimental properties, such as the behavior of the upper critical field.²⁹

The same type of model for Cooper pairing is likely to be relevant for the superconductivity in LaPt_3Si ($T_c \approx 0.67$ K), which has the same crystal structure as CePt_3Si . Experimental data of T_1^{-1} by NQR suggest a nodeless gap,³⁰ i.e., within our model $|\Psi| > |\Delta|$. These two compounds provide a neat pair of systems to be compared. In particular, CePt_3Si is a heavy fermion compound with magnetic order, while LaPt_3Si represents a much less correlated metal. It is now highly desirable to have further experimental confirmations of the pairing symmetry and hints for the pairing mechanisms at work in both materials.

Note added. After completing this work, we noted that a similar idea concerning the coexistence between the coherence effect in T_1^{-1} and the line node in a gap was briefly discussed in Ref. 31 by Fujimoto very recently. A further discussion of the low-temperature part of the NMR relaxation rate is given in Ref. 32 by Samokhin. However, our explanation of the peak in T_1^{-1} attributed to the coherence-effect term W_{FF} instead of W_{GG} is different from that of Ref. 32. The origin of the line-node gap due to the parity mixing discussed in this paper is different from both the propositions in Refs. 31 and 32.

We thank M. Yogi, Y. Kato, J. Goryo, D. F. Agterberg, A. Koga, and M. Matsumoto for helpful discussions. N.H. acknowledges support from the JSPS (2003 PFRA Program). We are also grateful for financial support from the Swiss Nationalfonds and the NCCR MaNEP.

¹V. M. Edelstein, Phys. Rev. Lett. **75**, 2004 (1995).

²L. P. Gor'kov and E. I. Rashba, Phys. Rev. Lett. **87**, 037004 (2001).

³P. A. Frigeri, D. F. Agterberg, A. Koga, and M. Sigrist, Phys. Rev. Lett. **92**, 097001 (2004); **93**, 099903(E) (2004).

⁴K. V. Samokhin, E. S. Zijlstra, and S. K. Bose, Phys. Rev. B **69**, 094514 (2004); **70**, 069902(E) (2004).

⁵I. A. Sergienko and S. H. Curnoe, Phys. Rev. B **70**, 214510 (2004).

⁶E. Bauer *et al.*, Phys. Rev. Lett. **92**, 027003 (2004).

⁷S. S. Saxena and P. Monthoux, Nature (London) **427**, 799 (2004).

⁸E. Bauer, I. Bonalde, and M. Sigrist, Fiz. Nizk. Temp. **31**, 984 (2005) [Low Temp. Phys. **31**, 748 (2005)].

⁹G. Dresselhaus, Phys. Rev. **100**, 580 (1955).

¹⁰E. I. Rashba, Fiz. Tverd. Tela (Leningrad) **1**, 407 (1959) [Sov. Phys. Solid State **1**, 368 (1959)].

¹¹L. N. Bulaevski, A. A. Guseinov, and A. I. Rusinov, Zh. Eksp. Teor. Fiz. **71**, 2356 (1976) [Sov. Phys. JETP **44**, 1243 (1976)].

¹²P. A. Frigeri, D. F. Agterberg, and M. Sigrist, New J. Phys. **6**, 115 (2004).

¹³M. Yogi, Y. Kitaoka, S. Hashimoto, T. Yasuda, R. Settai, T. D. Matsuda, Y. Haga, Y. Onuki, P. Rogl, and E. Bauer, Phys. Rev. Lett. **93**, 027003 (2004).

¹⁴E. Bauer, G. Hilscher, H. Michor, M. Sieberer, E. W. Scheidt, A. Griбанov, Yu. Seropegin, P. Rogl, A. Amato, W. Y. Song, J.-G. Park, D. T. Adroja, M. Nicklas, G. Sparn, M. Yogi, and Y. Kitaoka, Physica B **359-361**, 360 (2005).

¹⁵I. Bonalde, W. Brämer-Escamilla, and E. Bauer, Phys. Rev. Lett. **94**, 207002 (2005).

¹⁶K. Izawa, Y. Kasahara, Y. Matsuda, K. Behnia, T. Yasuda, R. Settai, and Y. Onuki, Phys. Rev. Lett. **94**, 197002 (2005).

¹⁷P. A. Frigeri, D. F. Agterberg, I. Milat, and M. Sigrist, cond-mat/0505108 (unpublished).

¹⁸P. W. Anderson, Phys. Rev. B **30**, 4000 (1984).

¹⁹G. Eilenberger, Z. Phys. **214**, 195 (1968).

²⁰A. I. Larkin and Yu. N. Ovchinnikov, Zh. Eksp. Teor. Fiz. **55**, 2262 (1968) [Sov. Phys. JETP **28**, 1200 (1969)].

²¹J. W. Serene and D. Rainer, Phys. Rep. **101**, 221 (1983).

²²N. Schopohl, J. Low Temp. Phys. **41**, 409 (1980).

²³C. T. Rieck, K. Scharnberg, and N. Schopohl, J. Low Temp. Phys. **84**, 381 (1991).

²⁴C. H. Choi and J. A. Sauls, Phys. Rev. B **48**, 13684 (1993).

²⁵H. Kusunose, Phys. Rev. B **70**, 054509 (2004).

²⁶N. Hayashi, K. Wakabayashi, P. A. Frigeri, and M. Sigrist, Phys. Rev. B **73**, 024504 (2006).

²⁷V. P. Mineev, Int. J. Mod. Phys. B **18**, 2963 (2004).

²⁸N. Hayashi and Y. Kato, Physica C **388-389**, 513 (2003).

²⁹R. P. Kaur, D. F. Agterberg, and M. Sigrist, Phys. Rev. Lett. **94**, 137002 (2005).

³⁰M. Yogi, Y. Kitaoka, S. Hashimoto, T. Yasuda, R. Settai, T. D. Matsuda, Y. Haga, Y. Onuki, P. Rogl, and E. Bauer, J. Phys. Chem. Solids (to be published).

³¹S. Fujimoto, Phys. Rev. B **72**, 024515 (2005).

³²K. V. Samokhin, Phys. Rev. B **72**, 054514 (2005).